No Emergency Brake: Slow Ocean Response to Abrupt Stratospheric Aerosol Injection

Daniel Pflüger[1], Claudia Elisabeth Wieners[1], Leo van Kampenhout[1], René Wijngaard[1], and Henk A. Dijkstra[2]

[1]Utrecht University
[2]Institute for Marine and Atmospheric research Utrecht

September 11, 2023

Abstract

Given the possibility of irreversible changes to the Earth system, technological interventions such as solar radiation management (SRM) are sometimes framed as possible climate emergency brakes. However, little knowledge exists on the efficacy of such disruptive interventions. To fill in this gap, we perform Community Earth System Model 2 (CESM 2) simulations of a SSP5-8.5 scenario on which we impose either gradual early-century SRM to stabilise surface temperatures or a rapid late-century cooling, both realised via stratospheric aerosol injection (SAI). While both scenarios cool Earth's surface, we find that ocean conditions differ drastically. The rapid-cooling scenario fails to dissipate sub-surface ocean heat content (OHC), ends up in a weaker AMOC state and does not restore an ailing North Atlantic deep convection. Furthermore, the weakened AMOC state mediates the climate response to rapid SAI, thus inducing an interhemispheric temperature asymmetry. Our results advise caution when considering SAI as an emergency intervention.

No Emergency Brake: Slow Ocean Response to Abrupt Stratospheric Aerosol Injection

Daniel Pflüger [1], Claudia E. Wieners[1], Leo van Kampenhout[1], René R. Wijngaard[1], Henk A. Dijkstra[1]

[1]Institute Marine and Atmospheric Research Utrecht, Princetonplein 5, 3584 CC Utrecht, The Netherlands

Key Points:

- Abrupt cooling via stratospheric aerosol injection (SAI) counteracts anthropogenic climate change mostly on a surface level in Community Earth System Model 2 (CESM 2) simulations
- Sub-surface ocean heat, weakened Atlantic Meridional Overturning Circulation (AMOC) and collapsed North Atlantic deep convection remain after intervention
- Decoupling of AMOC and GMST under abrupt SAI yields a climate state not seen in purely greenhouse-gas (GHG) forced simulations

Corresponding author: Daniel Pflüger, d.pfluger@uu.nl

Abstract

Given the possibility of irreversible changes to the Earth system, technological interventions such as solar radiation management (SRM) are sometimes framed as possible climate emergency brakes. However, little knowledge exists on the efficacy of such disruptive interventions. To fill in this gap, we perform Community Earth System Model 2 (CESM 2) simulations of a SSP5-8.5 scenario on which we impose either gradual early-century SRM to stabilise surface temperatures or a rapid late-century cooling, both realised via stratospheric aerosol injection (SAI). While both scenarios cool Earth's surface, we find that ocean conditions differ drastically. The rapid-cooling scenario fails to dissipate subsurface ocean heat content (OHC), ends up in a weaker AMOC state and does not restore an ailing North Atlantic deep convection. Furthermore, the weakened AMOC state mediates the climate response to rapid SAI, thus inducing an interhemispheric temperature asymmetry. Our results advise caution when considering SAI as an emergency intervention.

Plain Language Summary

Stratospheric aerosol injection (SAI) is a proposal to mask the effects of anthropogenic climate change by reflecting sunlight back into space. As such a large intervention may come along with physical and socio-political risks, SAI is sometimes framed as an 'emergency brake' to be deployed under the most dire of circumstances.

Using model simulations, we show that such an abrupt deployment fails to restore past climate conditions. While Earth's surface cools rapidly, the response is less definite in the ocean where reaction times are far longer. More specifically, rapid cooling only takes place on the ocean surface while deeper layers continue to trap excess heat. Additionally, important features of the ocean circulation and potential climate tipping elements do not quickly return to their pre-warming state. The combination of a cooled surface with an altered ocean circulation creates a novel, potentially undesirable, climate state.

Our study once again emphasizes the persistent impacts of greenhouse gas emissions. In particular, changes in inert systems, such as the ocean, act as a form of long-term debt which can not easily be redeemed. This cautions against the use of an emergency brake framing for SAI.

1 Introduction

While global heating puts increasing pressure on societies and ecosystems (IPCC, 2022a), current policies are insufficient to prevent 1.5°C or even 2°C of warming (IPCC, 2022b). To mitigate the associated risks, *Solar Radiation Management* (SRM) has been proposed as a complimentary measure to emission cuts (National Academies of Sciences, Engineering, and Medicine, 2021). Among several potential schemes, *Stratospheric Aerosol Injection* (SAI) received considerable attention due to its low perceived technical barriers (Smith, 2020) as well as its plausible physical effectiveness (Kleinschmitt et al., 2018; Plazzotta et al., 2018).

Even if global mean surface temperature (GMST) were kept constant using SRM, residual climate changes would still be present. Nevertheless, SRM would likely bring relevant climate variables closer to their pre-industrial state in many regions (Irvine et al., 2019). Besides these physical aspects, SRM has wide-reaching socio-political and ethical implications (Buck, 2019; Svoboda, 2017; Oomen, 2021) leading some to call for a ban on its research and deployment (Biermann et al., 2022) whereas others call for further scientific studies (Wieners et al., 2023).

Several scenarios of SRM governance and deployment have been suggested (Lockley et al., 2022; Barrett et al., 2014). For example, SRM might be used timely to reduce warming overshoot ("peak-shaving") or slow down the rate of warming (Florin et al., 2020). It can also be used reactively, e.g. to prevent a climate emergency or breaching a temperature limit (Crutzen, 2006) potentially under the assumption that SRM is invoked only if more acceptable options fall short ("emergency brake").

Climate model simulations typically assume SRM to be used immediately (Tilmes et al., 2018, 2019) or in the near future (MacMartin et al., 2017). Less attention has been paid to the question what would happen if SRM were deployed only after several decades of GHG-induced heating. This question is far from trivial. Even for identical greenhouse gas trajectories, it may be impossible to return from a world where SRM has started "late" to the state that would have been achieved if SRM had started earlier. Such a lack of reversibility might be temporary (early and late SRM eventually converge) or absolute (they never converge). Even a temporary lack of reversibility might have socio-economic and political repercussions and limit SRM's potential to act as an emergency brake.

Ocean processes involving long timescales could potentially bring about a temporary lack of reversibility. Such processes include changes in the ocean heat content (OHC) (Fasullo et al., 2018) and changes in the North Atlantic circulation such as a weakening of the Atlantic Meridional Overturning Circulation (AMOC) (Hassan et al., 2021; Schwinger et al., 2022) or the shutdown of deep convection (Sgubin et al., 2017; Swingedouw et al., 2021).

In this study, we ask how effective SAI would be as emergency brake, i.e. to what extent abruptly lowering GMST with aerosol-induced shading would reverse climate change, and how this implementation compares to a gradual, earlier deployment. Aforementioned ocean features are our main focus as we suspect long response timescales to give different outcomes depending on the SAI strategy.

2 Methods

We use the CMIP6 model CESM2 (Danabasoglu et al., 2020) with atmospheric component CAM6. While the configuration CESM2-WACCM is more comprehensive, it is also more computationally expensive. As CESM2-CAM6 lacks interactive stratospheric sulphate chemistry, we prescribe aerosol fields based on prior CESM2-WACCM simulations (Tilmes et al., 2019).

While our WACCM-derived aerosol fields have a fixed spatial and seasonal pattern, we can scale the overall amplitude of the forcing every year. This (single) degree of freedom is used to stabilise GMST at its target value of 1.5°C above pre-industrial conditions under a SSP5-8.5 scenario. More specifically, a feedforward-feedback controller (Kravitz et al., 2016, 2017) dynamically adjusts the aerosol burden in the stratosphere to target a specified GMST. Technical details are outlined in the supplementary material.

We simulate three scenarios based on SSP5-8.5 background emissions:

- Control (2015-2100): historical spin-up continued by SSP5-8.5
- SAI 2020 (gradual SAI): branch off from Control in 2020, stabilise GMST at a target value of 1.5° above pre-industrial conditions
- SAI 2080 (emergency brake): branch off from Control in 2080, deploy SAI to restore GMST to the same target as SAI 2020.

As our scenarios involve very high levels of GHG and aerosol forcing, they are intended as physical edge cases rather than realistic or desirable real-world scenarios. In that sense, SAI 2080 serves only as an upper boundary for the response to SRM-induced cooling.

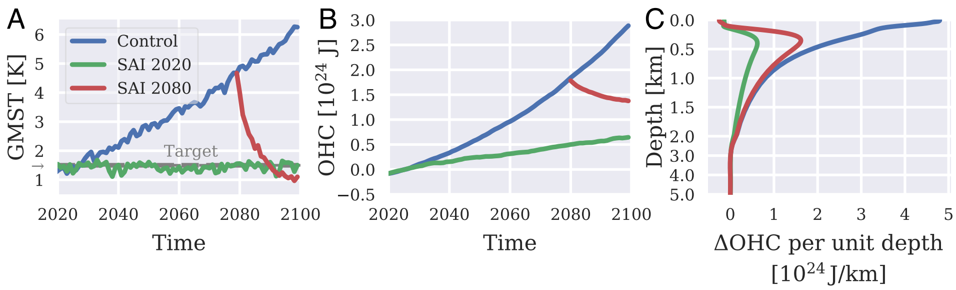

Figure 1. **A**: Annual mean GMST above pre-industrial reference temperature **B**: Change in annual mean total depth OHC relative to 2020-2030 conditions in Control. **C**: Difference in vertical OHC between end-of-simulation (2090-2100) conditions and present-day conditions in Control.

3 Results

3.1 Temperature Response

In Fig. 1A, we see that the gradual SAI strategy (SAI 2020) indeed stabilises GMST at target level. By contrast, SAI 2080 experiences rapid cooling. The latter can be reduced by tuning the feedback procedure (see Fig. S1).

Even though GMST is stabilised, total depth OHC accumulates continuously in SAI 2020 (Fig.1B) in agreement with a past study (Fasullo et al., 2018). The warming takes place below the surface and is likely a consequence of deep ocean response timescales (Cheng et al., 2022) in combination with the feedback controller. As sub-surface layers have not yet adapted to increased surface temperatures, they act as a heat sink for the ocean surface. The induced downward heat flux is then compensated by the feedback controller that allows for some top-of-atmosphere radiative imbalance in order to stabilize GMST.

SAI 2080 accumulates more total depth OHC than SAI 2020. The sub-surface vertical OHC distribution of SAI 2080 (Fig.1C) matches that of Control. On the surface, however, both SAI scenarios have comparable OHC anomalies. This suggests that while abrupt SAI readily cools the ocean surface, heat anomalies trapped in deeper layers are more persistent.

Surface temperature responses to SAI are spatially inhomogeneous (Fig. 2). Most strikingly, the subpolar North Atlantic is significantly overcooled in both SAI scenarios. This pattern resembles an intensified *North Atlantic Warming Hole* known from purely GHG-forced simulations (Drijfhout et al., 2012; Menary & Wood, 2018), which to some extent is also visible in Control. While the strong overcooling is limited to the warming hole in SAI 2020, SAI 2080 shows a large-scale overcooling covering most of the Northern Hemisphere, while the Southern Hemisphere remains warmer than in SAI 2020.

Multi-objective feedback procedures (Kravitz et al., 2017; MacMartin et al., 2017) allow for a more elaborate control of the global temperature pattern including the interhemispheric temperature gradient. Therefore, the asymmetric response of SAI 2080 (Fig. 2E) may be mitigated in a refined control scheme. In our study, however, both SAI scenarios use spatially identical aerosol patterns with a single degree of freedom which rules out a control of the asymmetry.

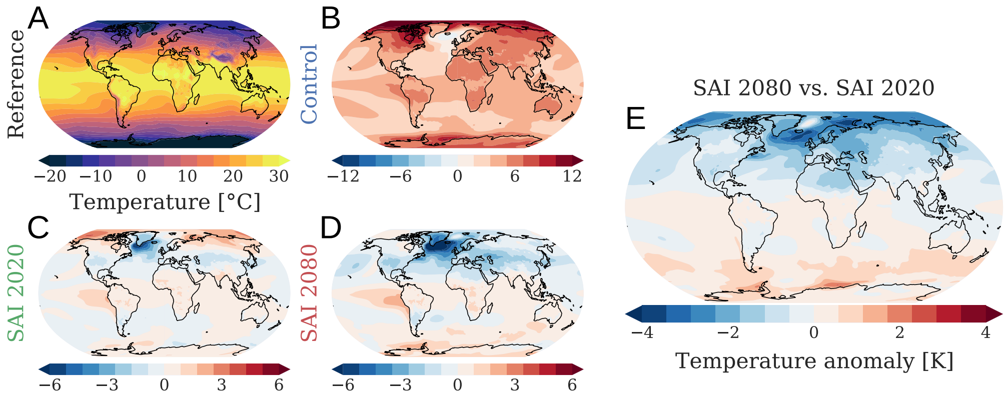

Figure 2. **A**: Reference (2020-2030) annual mean near-surface air temperatures in Control **B-D**: Late-century (2090-2100) temperature changes with respect to the reference for Control, SAI 2020 and SAI 2080 respectively. **E**: Difference between SAI scenarios (**D** minus **C**)

3.2 AMOC Response

The AMOC index and meridional heat transport (MHT) roughly halve in Control (Fig. 3A-B). Even the CMIP6 low-emission SSP1-2.6 scenario is projected to lead to similar AMOC index changes. SAI 2020 drastically mitigates but does not halt the AMOC and MHT decline. SAI 2080 stabilizes the AMOC index but only has an inconclusive impact on the MHT.

Interestingly, SAI effectively decouples the GMST and the AMOC index (Fig. 3C). This could explain the interhemispheric temperature contrast featured in SAI 2080: a weak AMOC impedes northward heat transport leading to a see-saw temperature pattern (Stocker, 1998; Liu et al., 2020) that is not masked by heat otherwise present in Control.

To study the spatial pattern of the AMOC, we plot meridional streamfunction changes under all scenarios from 2070-2080 to 2090-2100 (Fig. 4). This choice of time intervals helps to reveal the immediate AMOC response to SAI 2080. Additionally, we subtract the changes in Control from the ones in the SAI scenarios in an attempt to disentangle GHG from SAI-related impacts.

Fig. 4D reveals a potential feedback in the AMOC stabilization under SAI 2080. Following the deployment, the pattern of relative AMOC strengthening closely mirrors the pre-deployment streamfunction, albeit mostly near the surface and in the northern hemisphere. This suggests that the AMOC response to abrupt SAI is dependent on the AMOC state itself. While a similar observation can be made for SAI 2020 (Fig. 4C), disentangling the forced response from internal feedback is not obvious during the gradual change in aerosol forcing. SAI 2080 gives a much better indication that it is indeed the state of the AMOC which steers its response to SAI.

This result again highlights the lack of immediate climate reversibility under SAI. A weakened AMOC state likely presents an obstacle to a SAI-based stabilization or recovery.

3.3 North Atlantic Deep Convection

We now focus on deep convection processes in the North Atlantic. Using mixed layer depth as a proxy for deep convection, we identify two regions, *East* and *West*, where the

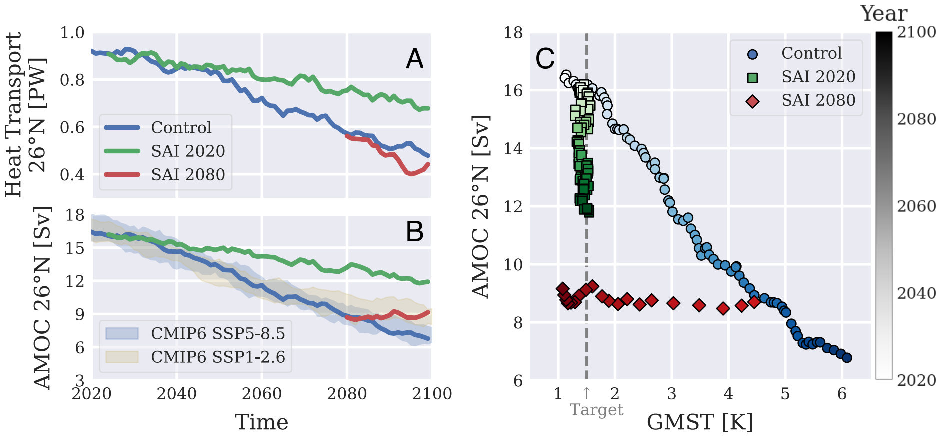

Figure 3. **A**: Annual mean Atlantic northwards heat transport at 26° N where we apply a rolling average over five year periods with backward window **B**: AMOC index defined as the maximum of the annual mean meridional overturning streamfunction at 26° N below 200 m - Partially transparent uncertainty bands depict three CESM2 CMIP6 ensemble members (Danabasoglu, 2019a, 2019b) per GHG concentration pathway. The uncertainty is the ensemble standard deviation. Again, we apply rolling averages over five year periods. **C**: Annual mean GMST vs. AMOC index - The marker saturation denotes the year: light (2020) to dark (2100).

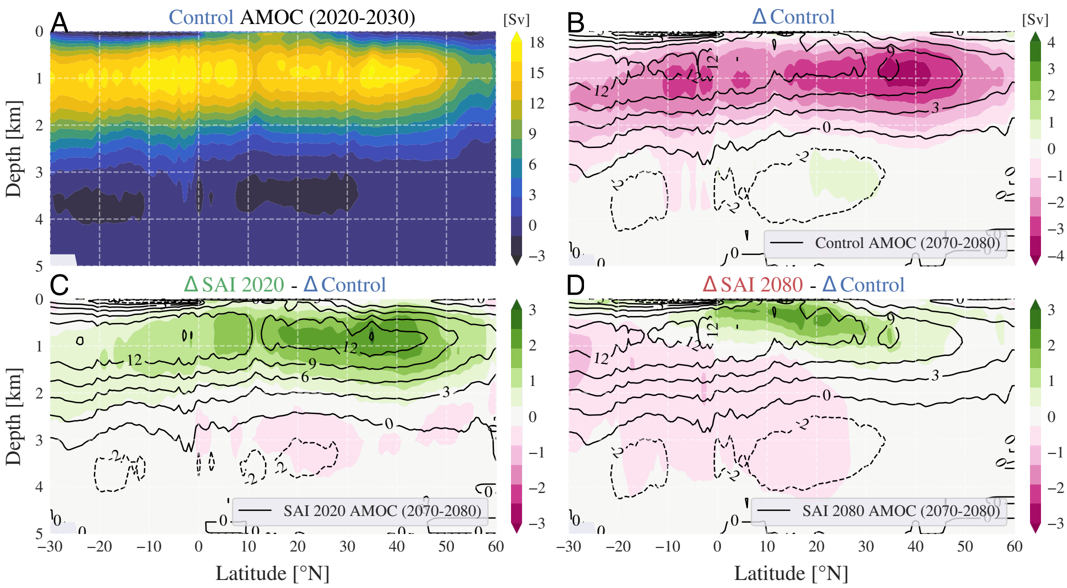

Figure 4. **A**: AMOC streamfunction in Control averaged over 2020-2030. In **B-D**, for any simulation X, Δ X is the mean over 2090-2100 minus the mean over 2070-2080. **B**: Change in AMOC streamfunction under Control - Black contour lines show the mean streamfunction over 2070-2080 for Control while the shading indicates Δ Control. **C**: Change in AMOC streamfunction in SAI 2020 relative to Control - Black contour lines show the mean streamfunction over 2070-2080 for SAI 2020 while the shading indicates Δ SAI 2020 - Δ Control. **D**: Analogous to **C** but for SAI 2080.

mixed layer depth in April (the month with the deepest mixed layer) exceeds 550 m (Fig. 5A). This threshold depth was chosen as it is sufficiently large to distinguish deep convection from regular mixed-layer conditions and small enough to provide a good signal-to-noise ratio. The regions are separated longitudinally by the southern tip of Greenland.

In Control, deep convection in *West* ceases around 2050, followed by a shutdown in *East* around 2060. SAI 2020 prevents the shutdown in *East*, but only postpones the shutdown in *West* by about a decade. The *West* shutdown is not as definite as in the case of Control and isolated years with deep convection still occur. For SAI 2080, deep convection remains absent in both regions with the exception of a single outlier year for *East*.

Why does cooling in SAI 2080 not revive deep convection? We address this question by studying the ocean stratification over both deep convection regions. Deep convection in April is inhibited if the surface density in the previous September has been too low, i.e. the water column is too stratified (Fig. S3). Thus, surface density serves as a proxy for favorable convection conditions.

The sea surface density is determined by temperature and salinity, also seen in Fig. 5. In all scenarios, final salinities are well below reference conditions. SAI 2020 roughly halves the decline with respect to Control. This difference becomes very noticeable mid-century simultaneously with the *East* and *West* shutdown in Control. SAI 2080 does not fundamentally alter the trajectory of Control apart from a transient increase in salinity that correlates with an isolated year of deep convection. Therefore, freshening contributes to density loss in all scenarios.

Temperature trends are rather complex in the case of Control (Fig. 5D-F.). An initial phase of slight cooling is interspersed with rapid, intense variability mid-century and finally succeeded by warming. Multiple factors like GHG-induced heating, cooling from a declining AMOC as well as convection related surfaces fluxes and currents overlap and are causing this behaviour.

SAI 2020 shows an overall cooling trend dominated by a quick decline at time of *West* shutdown. In SAI 2080, prior deep convection shutdown combined with SAI leads to drastic cooling even falling below SAI 2020 levels (Fig. 5D). These temperature drops have a positive effect on density and thereby convection. Still, the dramatic cooling in SAI 2080 does not elevate densities to SAI 2020 levels (Fig. 5F). Therefore, the salinity deficit of SAI 2080 with respect to SAI 2080 (Fig. 5E) presents a clear obstacle for restarting deep convection.

Our results can be explained in terms of multiple physical drivers. Firstly, all scenarios see an increase in surface freshwater forcing (Fig. S2) which contributes to a gradual salinity loss. This weakens convection and consequently the AMOC. Subsequently, weak AMOC and convection conditions lead to less salt transport into the subpolar gyre, hence reinforcing the salinity decline (Kuhlbrodt et al., 2007). This is particularly true for the late years of Control and SAI 2080. Finally, increasing the surface density via cooling has 'diminishing returns': density gains are less than proportional to temperature decreases owing to the nonlinear properties of sea water density. As shown in the supplementary material (Fig. S4), this further reduces the efficacy of SAI 2080.

To summarise, SAI 2020 partially stabilizes deep convection. In contrast, the salinity deficit accumulated up to deployment time in SAI 2080 becomes an obstacle for strengthening convection. There, the absence of positive convective feedback combined with a weak AMOC offers little hope of a decisive recovery but internal variability may still lead to isolated events of deep convection. It is not implausible that multiple such events could compound and eventually restore deep convection in the longer term.

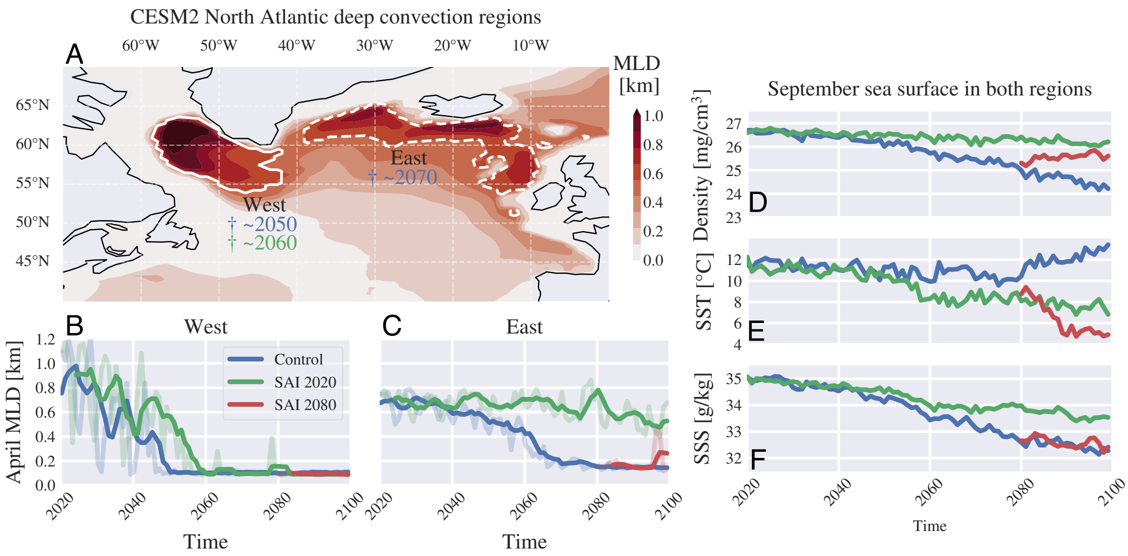

Figure 5. **A**: North Atlantic April mixed layer depths in CESM2 (2020-2030) - *East* and *West* are enclosed by solid and dashed lines respectively. Shutdown dates are denoted with a cross and colored according to scenario (blue: Control, green: SAI 2020). **B-C**: April mixed layer depths in *West* and *East* respectively - Solid lines are five year rolling means (with backward window) applied to the data shown by transparent lines. **D-F**: September mean sea surface density, temperature and salinity over the total *East* and *West* region

4 Discussion

In our simulations, the quick drop in GMST due to abrupt SAI is contrasted by a slow ocean response. Gradual SAI, on the other hand, retains an ocean state much closer to the present-day reference. Elevated OHC, weak AMOC and absent deep convection coupled with a lower GMST presents a (transient) climate state unknown from purely GHG-forced scenarios.

Note that our scenarios are extreme cases with a high signal-to-noise ratio, rather than desirable or plausible futures. More cautious protocols typically deploy SAI in tandem with emission mitigation to limit a temporary temperature overshoot (National Academies of Sciences, Engineering, and Medicine, 2021). If a cooling scenario were actually considered, a ramp-up of SAI would be more sensible than the sudden deployment in SAI 2080. Such a gradual approach would enable a fine-tuning of the injection scheme based on observations.

Besides the high forcings, our scenarios also involve a limited SAI scheme. As our implementation relies on a single degree of freedom, we can only meet a GMST target but not control other aspects of the temperature pattern. More control parameters, on the other hand, may be beneficial to prevent a interhemispheric temperature asymmetry which risks a displacement of the ITCZ (Broccoli et al., 2006; Bischoff & Schneider, 2016). Still, restoring the meridional temperature pattern in SAI 2080 would come with problems of its own: less cooling over the North Atlantic further endangers deep convection.

As for our results, a mitigating effect of SAI on AMOC decline was already known in multiple models (Tilmes et al., 2018, 2019; Xie et al., 2022) but not in the case of late-century abrupt deployment. Similarly, the impaired effectiveness of abrupt SAI on reducing OHC is a new result. To our knowledge, no studies have been performed on the effect of SAI on deep convection shutdown either. Regarding this aspect, model dependencies are certain as deep convection shutdown is not a universal phenomenon in CMIP6 (Swingedouw et al., 2021).

It is worth pointing out similarities between our abrupt SAI case and rapid negative emission scenarios (Schwinger et al., 2022). Removal of GHG after prolonged heating can lead to an interhemispheric temperature asymmetry if the timescale of extraction is shorter than that of the AMOC recovery. Therefore, the possibility of SAI to manage the interhemispheric temperature gradient is an advantage compared to GHG removal.

A major questions remains open: do the climates of both SAI scenarios eventually converge? This question cannot be answered without extending the simulations, which is outside the scope of this study. When extrapolating our results, the OHC difference is expected to lessen due to residual ocean warming in SAI 2020. Whether the gap fully closes may also depend on the AMOC and deep convection because of their impact on ocean heat uptake (Marshall & Zanna, 2014). As for deep convection, the aforementioned salinity deficit in SAI 2080 inhibits convergence of the SAI scenarios. Nevertheless, should some years of deep convection arise in SAI 2080 (e.g. as a result of natural variability), salt import would be strengthened, thereby improving long-term prospects for deep convection.

5 Summary

In this study, we presented model results of a late-century “emergency brake” SAI deployment that aims to restore surface temperatures under simultaneous GHG forcing. By comparing our findings with a gradual early-century SAI scenario, we show that abrupt late-century SAI is less effective at mitigating changes in OHC, the AMOC and North Atlantic deep convection.

Firstly, abrupt SAI failed to release heat trapped in deeper ocean layers. Even an early onset of SAI only mitigates but does not halt OHC accumulation. Both results are linked to slow ocean equilibration times.

Secondly, abrupt SAI partially stabilized a weakened AMOC, albeit not halting the decline of northward heat transport. Under earlier SAI, the AMOC decline is mitigated in both, volume and heat transport. As a result, the scenarios achieved drastically different AMOC states despite comparable GMST. A weaker AMOC may contribute to the observed overcooling of the northern hemisphere in the emergency brake scenario. This, in turn, may be relevant for the choice of injection pattern.

Thirdly, a shutdown of North Atlantic deep convection could not be reversed with rapid, SAI-induced cooling. We suspect that a weakened AMOC, absence of convective feedback, fresher surface conditions as well as non-linear properties of water density pose an obstacle for restarting deep convection. An early intervention, on the other hand, retains more salt in the North Atlantic, hence the partial stabilization of deep convection.

All these findings suggest that SAI is not an effective emergency brake. Ocean changes induced by anthropogenic climate change can persist despite a rapid lowering of GMST. That is why, if SAI were ever considered, its efficacy would be limited by the ocean changes already locked-in. To avoid facing the choice of whether and how to deploy SAI all together, further climate change must be mitigated by curbing GHG emissions.

6 Open Research

The code for our SAI protocol will be shared upon reasonable request.

The CMIP6 data used for comparison in Fig. 3 is publicly available (Danabasoglu, 2019a, 2019b).

Acknowledgments

We thank Daniele Visioni, Doug McMartin and Ben Kravitz for sharing their feedforward-feedback controller code, our colleague Michael Kliphuis for providing his AMOC streamfunction tools, Simone Tilmes for providing CESM2-WACCM data. Furthermore, we thank Jasper de Jong and Michiel Baatsen for fruitful discussions on the feedback control of SAI 2080.

References

Barrett, S., Lenton, T. M., Millner, A., Tavoni, A., Carpenter, S., Anderies, J. M., ... De Zeeuw, A. (2014). Climate engineering reconsidered. *Nature Climate Change*. doi: 10.1038/nclimate2278

Biermann, F., Oomen, J., Gupta, A., Ali, S. H., Conca, K., Hajer, M. A., ... VanDeveer, S. D. (2022). Solar geoengineering: The case for an international non-use agreement. *WIREs Climate Change*. doi: 10.1002/wcc.754

Bischoff, T., & Schneider, T. (2016). The equatorial energy balance, ITCZ position, and double-ITCZ bifurcations. *Journal of Climate*. doi: 10.1175/JCLI-D-15-0328.1

Broccoli, A. J., Dahl, K. A., & Stouffer, R. J. (2006). Response of the ITCZ to northern hemisphere cooling. *Geophysical Research Letters*. doi: 10.1029/2005GL024546

Buck, H. J. (2019). *After geoengineering: climate tragedy, repair, and restoration.* Verso.

Cheng, L., Von Schuckmann, K., Abraham, J. P., Trenberth, K. E., Mann, M. E., Zanna, L., ... Lin, X. (2022). Past and future ocean warming. *Nature Reviews Earth & Environment*. doi: 10.1038/s43017-022-00345-1

Crutzen, P. J. (2006). Albedo enhancement by stratospheric sulfur injections: A contribution to resolve a policy dilemma? *Climatic Change*. doi: 10.1007/s10584-006-9101-y

Danabasoglu, G. (2019a). *NCAR CESM2 model output prepared for CMIP6 ScenarioMIP ssp370.* Earth System Grid Federation. doi: 10.22033/ESGF/CMIP6.7753

Danabasoglu, G. (2019b). *NCAR CESM2 model output prepared for CMIP6 ScenarioMIP ssp585.* Earth System Grid Federation. doi: 10.22033/ESGF/CMIP6.7768

Danabasoglu, G., Lamarque, J., Bacmeister, J., Bailey, D. A., DuVivier, A. K., Edwards, J., ... Strand, W. G. (2020). The community earth system model version 2 (CESM2). *Journal of Advances in Modeling Earth Systems*. doi: 10.1029/2019MS001916

Drijfhout, S., van Oldenborgh, G. J., & Cimatoribus, A. (2012). Is a decline of AMOC causing the warming hole above the north atlantic in observed and modeled warming patterns? *Journal of Climate*. doi: 10.1175/JCLI-D-12-00490.1

Fasullo, J. T., Tilmes, S., Richter, J. H., Kravitz, B., MacMartin, D. G., Mills, M. J., & Simpson, I. R. (2018). Persistent polar ocean warming in a strategically geoengineered climate. *Nature Geoscience*. doi: 10.1038/s41561-018-0249-7

Florin, M.-V., Rouse, P., Hubert, A.-M., Honegger, M., & Reynolds, J. (2020). lnternational governance issues on climate engineering information for policymakers. doi: 10.5075/EPFL-IRGC-277726

Hassan, T., Allen, R. J., Liu, W., & Randles, C. A. (2021). Anthropogenic aerosol forcing of the atlantic meridional overturning circulation and the associated mechanisms in CMIP6 models. *Atmospheric Chemistry and Physics*. doi: 10.5194/acp-21-5821-2021

IPCC. (2022a). *Climate change 2022: Impacts, adaptation and vulnerability.* Cambridge University Press. doi: 10.1017/9781009325844

IPCC. (2022b). *Climate change 2022: Mitigation of climate change.* Cambridge University Press.

Irvine, P., Emanuel, K., He, J., Horowitz, L. W., Vecchi, G., & Keith, D. (2019). Halving warming with idealized solar geoengineering moderates key climate hazards. *Nature Climate Change*. doi: 10.1038/s41558-019-0398-8

Kleinschmitt, C., Boucher, O., & Platt, U. (2018). Sensitivity of the radiative forcing by stratospheric sulfur geoengineering to the amount and strategy of the SO_2 injection studied with the LMDZ-S3A model. *Atmospheric Chemistry and Physics*. doi: 10.5194/acp-18-2769-2018

Kravitz, B., MacMartin, D. G., Mills, M. J., Richter, J. H., Tilmes, S., Lamarque, J., ... Vitt, F. (2017). First simulations of designing stratospheric sulfate aerosol geoengineering to meet multiple simultaneous climate objectives. *Journal of Geophysical Research: Atmospheres*. doi: 10.1002/2017JD026874

Kravitz, B., MacMartin, D. G., Wang, H., & Rasch, P. J. (2016). Geoengineering as a design problem. *Earth System Dynamics*. doi: 10.5194/esd-7-469-2016

Kuhlbrodt, T., Griesel, A., Montoya, M., Levermann, A., Hofmann, M., & Rahmstorf, S. (2007). On the driving processes of the atlantic meridional overturning circulation. *Reviews of Geophysics*.

Liu, W., Fedorov, A. V., Xie, S.-P., & Hu, S. (2020). Climate impacts of a weakened atlantic meridional overturning circulation in a warming climate. *Science Advances*. doi: 10.1126/sciadv.aaz4876

Lockley, A., Xu, Y., Tilmes, S., Sugiyama, M., Rothman, D., & Hindes, A. (2022). 18 politically relevant solar geoengineering scenarios. *Socio-Environmental Systems Modelling*. doi: 10.18174/sesmo.18127

MacMartin, D. G., Kravitz, B., Tilmes, S., Richter, J. H., Mills, M. J., Lamarque, J., ... Vitt, F. (2017). The climate response to stratospheric aerosol geoengineering can be tailored using multiple injection locations. *Journal of Geophysical Research: Atmospheres*. doi: 10.1002/2017JD026868

Marshall, D. P., & Zanna, L. (2014). A conceptual model of ocean heat uptake under climate change. *Journal of Climate*. doi: 10.1175/JCLI-D-13-00344.1

Menary, M. B., & Wood, R. A. (2018). An anatomy of the projected north atlantic warming hole in CMIP5 models. *Climate Dynamics*. doi: 10.1007/s00382-017-3793-8

National Academies of Sciences, Engineering, and Medicine. (2021). *Reflecting sunlight: Recommendations for solar geoengineering research and research governance.* National Academies Press. doi: 10.17226/25762

Oomen, J. (2021). *Imagining climate engineering: dreaming of the designer climate.* Routledge, Taylor & Francis Group.

Plazzotta, M., Séférian, R., Douville, H., Kravitz, B., & Tjiputra, J. (2018). Land surface cooling induced by sulfate geoengineering constrained by major volcanic eruptions. *Geophysical Research Letters*. doi: 10.1029/2018GL077583

Schwinger, J., Asaadi, A., Goris, N., & Lee, H. (2022). Possibility for strong northern hemisphere high-latitude cooling under negative emissions. *Nature Communications*. doi: 10.1038/s41467-022-28573-5

Sgubin, G., Swingedouw, D., Drijfhout, S., Mary, Y., & Bennabi, A. (2017). Abrupt cooling over the north atlantic in modern climate models. *Nature Communications*. doi: 10.1038/ncomms14375

Smith, W. (2020). The cost of stratospheric aerosol injection through 2100. *Environmental Research Letters*. doi: 10.1088/1748-9326/aba7e7

Stocker, T. F. (1998). The seesaw effect. *Science*. doi: 10.1126/science.282.5386.61

Svoboda, T. (2017). *The ethics of climate engineering: solar radiation management and non-ideal justice*. Routledge, Taylor & Francis Group.

Swingedouw, D., Bily, A., Esquerdo, C., Borchert, L. F., Sgubin, G., Mignot, J., & Menary, M. (2021). On the risk of abrupt changes in the north atlantic subpolar gyre in CMIP6 models. *Annals of the New York Academy of Sciences*. doi: 10.1111/nyas.14659

Tilmes, S., MacMartin, D. E., Lenaerts, J. T. M., Van Kampenhout, L., Muntjewerf, L., Xia, L., … Robock, A. (2019). Reaching 1.5 °c and 2.0 °c global surface temperature targets using stratospheric aerosol geoengineering [preprint]. *Earth System Dynamics*. doi: 10.5194/esd-2019-76

Tilmes, S., Richter, J. H., Kravitz, B., MacMartin, D. G., Mills, M. J., Simpson, I. R., … Ghosh, S. (2018). CESM1(WACCM) stratospheric aerosol geoengineering large ensemble project. *Bulletin of the American Meteorological Society*. doi: 10.1175/BAMS-D-17-0267.1

Wieners, C. E., Hofbauer, B. P., De Vries, I. E., Honegger, M., Visioni, D., Russchenberg, H. W. J., & Felgenhauer, T. (2023). Solar radiation modification is risky, but so is rejecting it: a call for balanced research. *Oxford Open Climate Change*. doi: 10.1093/oxfclm/kgad002

Xie, M., Moore, J. C., Zhao, L., Wolovick, M., & Muri, H. (2022). Impacts of three types of solar geoengineering on the atlantic meridional overturning circulation. *Atmospheric Chemistry and Physics*. doi: 10.5194/acp-22-4581-2022

No Emergency Brake: Slow Ocean Response to Abrupt Stratospheric Aerosol Injection

Daniel Pflüger [1],Claudia E. Wieners[1], Leo van Kampenhout[1], René R. Wijngaard[1], Henk A. Dijkstra[1]

[1]Institute Marine and Atmospheric Research Utrecht, Princetonplein 5, 3584 CC Utrecht, The Netherlands

Key Points:

- Abrupt cooling via stratospheric aerosol injection (SAI) counteracts anthropogenic climate change mostly on a surface level in Community Earth System Model 2 (CESM 2) simulations
- Sub-surface ocean heat, weakened Atlantic Meridional Overturning Circulation (AMOC) and collapsed North Atlantic deep convection remain after intervention
- Decoupling of AMOC and GMST under abrupt SAI yields a climate state not seen in purely greenhouse-gas (GHG) forced simulations

Corresponding author: Daniel Pflüger, `d.pfluger@uu.nl`

Abstract

Given the possibility of irreversible changes to the Earth system, technological interventions such as solar radiation management (SRM) are sometimes framed as possible climate emergency brakes. However, little knowledge exists on the efficacy of such disruptive interventions. To fill in this gap, we perform Community Earth System Model 2 (CESM 2) simulations of a SSP5-8.5 scenario on which we impose either gradual early-century SRM to stabilise surface temperatures or a rapid late-century cooling, both realised via stratospheric aerosol injection (SAI). While both scenarios cool Earth's surface, we find that ocean conditions differ drastically. The rapid-cooling scenario fails to dissipate subsurface ocean heat content (OHC), ends up in a weaker AMOC state and does not restore an ailing North Atlantic deep convection. Furthermore, the weakened AMOC state mediates the climate response to rapid SAI, thus inducing an interhemispheric temperature asymmetry. Our results advise caution when considering SAI as an emergency intervention.

Plain Language Summary

Stratospheric aerosol injection (SAI) is a proposal to mask the effects of anthropogenic climate change by reflecting sunlight back into space. As such a large intervention may come along with physical and socio-political risks, SAI is sometimes framed as an 'emergency brake' to be deployed under the most dire of circumstances.

Using model simulations, we show that such an abrupt deployment fails to restore past climate conditions. While Earth's surface cools rapidly, the response is less definite in the ocean where reaction times are far longer. More specifically, rapid cooling only takes place on the ocean surface while deeper layers continue to trap excess heat. Additionally, important features of the ocean circulation and potential climate tipping elements do not quickly return to their pre-warming state. The combination of a cooled surface with an altered ocean circulation creates a novel, potentially undesirable, climate state.

Our study once again emphasizes the persistent impacts of greenhouse gas emissions. In particular, changes in inert systems, such as the ocean, act as a form of long-term debt which can not easily be redeemed. This cautions against the use of an emergency brake framing for SAI.

1 Introduction

While global heating puts increasing pressure on societies and ecosystems (IPCC, 2022a), current policies are insufficient to prevent 1.5°C or even 2°C of warming (IPCC, 2022b). To mitigate the associated risks, *Solar Radiation Management* (SRM) has been proposed as a complimentary measure to emission cuts (National Academies of Sciences, Engineering, and Medicine, 2021). Among several potential schemes, *Stratospheric Aerosol Injection* (SAI) received considerable attention due to its low perceived technical barriers (Smith, 2020) as well as its plausible physical effectiveness (Kleinschmitt et al., 2018; Plazzotta et al., 2018).

Even if global mean surface temperature (GMST) were kept constant using SRM, residual climate changes would still be present. Nevertheless, SRM would likely bring relevant climate variables closer to their pre-industrial state in many regions (Irvine et al., 2019). Besides these physical aspects, SRM has wide-reaching socio-political and ethical implications (Buck, 2019; Svoboda, 2017; Oomen, 2021) leading some to call for a ban on its research and deployment (Biermann et al., 2022) whereas others call for further scientific studies (Wieners et al., 2023).

Several scenarios of SRM governance and deployment have been suggested (Lockley et al., 2022; Barrett et al., 2014). For example, SRM might be used timely to reduce warming overshoot ("peak-shaving") or slow down the rate of warming (Florin et al., 2020). It can also be used reactively, e.g. to prevent a climate emergency or breaching a temperature limit (Crutzen, 2006) potentially under the assumption that SRM is invoked only if more acceptable options fall short ("emergency brake").

Climate model simulations typically assume SRM to be used immediately (Tilmes et al., 2018, 2019) or in the near future (MacMartin et al., 2017). Less attention has been paid to the question what would happen if SRM were deployed only after several decades of GHG-induced heating. This question is far from trivial. Even for identical greenhouse gas trajectories, it may be impossible to return from a world where SRM has started "late" to the state that would have been achieved if SRM had started earlier. Such a lack of reversibility might be temporary (early and late SRM eventually converge) or absolute (they never converge). Even a temporary lack of reversibility might have socio-economic and political repercussions and limit SRM's potential to act as an emergency brake.

Ocean processes involving long timescales could potentially bring about a temporary lack of reversibility. Such processes include changes in the ocean heat content (OHC) (Fasullo et al., 2018) and changes in the North Atlantic circulation such as a weakening of the Atlantic Meridional Overturning Circulation (AMOC) (Hassan et al., 2021; Schwinger et al., 2022) or the shutdown of deep convection (Sgubin et al., 2017; Swingedouw et al., 2021).

In this study, we ask how effective SAI would be as emergency brake, i.e. to what extent abruptly lowering GMST with aerosol-induced shading would reverse climate change, and how this implementation compares to a gradual, earlier deployment. Aforementioned ocean features are our main focus as we suspect long response timescales to give different outcomes depending on the SAI strategy.

2 Methods

We use the CMIP6 model CESM2 (Danabasoglu et al., 2020) with atmospheric component CAM6. While the configuration CESM2-WACCM is more comprehensive, it is also more computationally expensive. As CESM2-CAM6 lacks interactive stratospheric sulphate chemistry, we prescribe aerosol fields based on prior CESM2-WACCM simulations (Tilmes et al., 2019).

While our WACCM-derived aerosol fields have a fixed spatial and seasonal pattern, we can scale the overall amplitude of the forcing every year. This (single) degree of freedom is used to stabilise GMST at its target value of 1.5°C above pre-industrial conditions under a SSP5-8.5 scenario. More specifically, a feedforward-feedback controller (Kravitz et al., 2016, 2017) dynamically adjusts the aerosol burden in the stratosphere to target a specified GMST. Technical details are outlined in the supplementary material.

We simulate three scenarios based on SSP5-8.5 background emissions:

- Control (2015-2100): historical spin-up continued by SSP5-8.5
- SAI 2020 (gradual SAI): branch off from Control in 2020, stabilise GMST at a target value of 1.5° above pre-industrial conditions
- SAI 2080 (emergency brake): branch off from Control in 2080, deploy SAI to restore GMST to the same target as SAI 2020.

As our scenarios involve very high levels of GHG and aerosol forcing, they are intended as physical edge cases rather than realistic or desirable real-world scenarios. In that sense, SAI 2080 serves only as an upper boundary for the response to SRM-induced cooling.

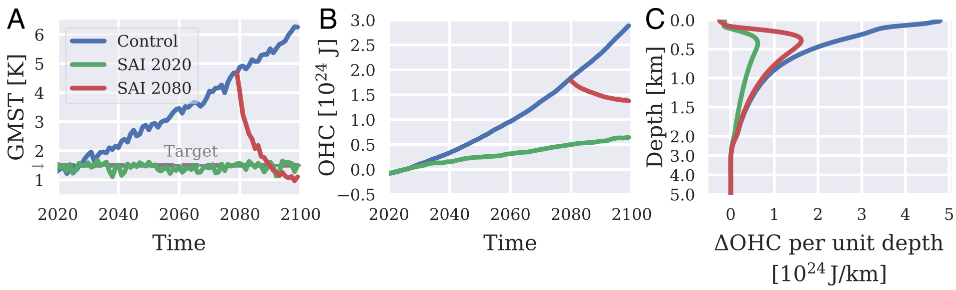

Figure 1. **A**: Annual mean GMST above pre-industrial reference temperature **B**: Change in annual mean total depth OHC relative to 2020-2030 conditions in Control. **C**: Difference in vertical OHC between end-of-simulation (2090-2100) conditions and present-day conditions in Control.

3 Results

3.1 Temperature Response

In Fig. 1A, we see that the gradual SAI strategy (SAI 2020) indeed stabilises GMST at target level. By contrast, SAI 2080 experiences rapid cooling. The latter can be reduced by tuning the feedback procedure (see Fig. S1).

Even though GMST is stabilised, total depth OHC accumulates continuously in SAI 2020 (Fig.1B) in agreement with a past study (Fasullo et al., 2018). The warming takes place below the surface and is likely a consequence of deep ocean response timescales (Cheng et al., 2022) in combination with the feedback controller. As sub-surface layers have not yet adapted to increased surface temperatures, they act as a heat sink for the ocean surface. The induced downward heat flux is then compensated by the feedback controller that allows for some top-of-atmosphere radiative imbalance in order to stabilize GMST.

SAI 2080 accumulates more total depth OHC than SAI 2020. The sub-surface vertical OHC distribution of SAI 2080 (Fig.1C) matches that of Control. On the surface, however, both SAI scenarios have comparable OHC anomalies. This suggests that while abrupt SAI readily cools the ocean surface, heat anomalies trapped in deeper layers are more persistent.

Surface temperature responses to SAI are spatially inhomogeneous (Fig. 2). Most strikingly, the subpolar North Atlantic is significantly overcooled in both SAI scenarios. This pattern resembles an intensified *North Atlantic Warming Hole* known from purely GHG-forced simulations (Drijfhout et al., 2012; Menary & Wood, 2018), which to some extent is also visible in Control. While the strong overcooling is limited to the warming hole in SAI 2020, SAI 2080 shows a large-scale overcooling covering most of the Northern Hemisphere, while the Southern Hemisphere remains warmer than in SAI 2020.

Multi-objective feedback procedures (Kravitz et al., 2017; MacMartin et al., 2017) allow for a more elaborate control of the global temperature pattern including the interhemispheric temperature gradient. Therefore, the asymmetric response of SAI 2080 (Fig. 2E) may be mitigated in a refined control scheme. In our study, however, both SAI scenarios use spatially identical aerosol patterns with a single degree of freedom which rules out a control of the asymmetry.

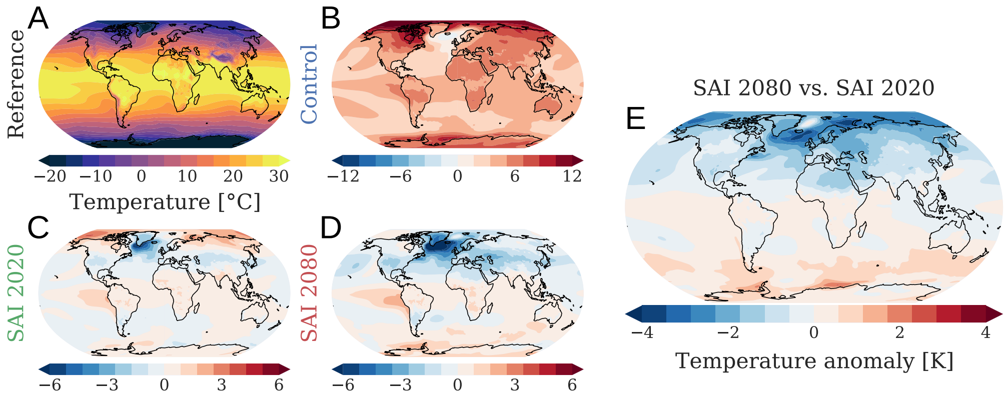

Figure 2. **A**: Reference (2020-2030) annual mean near-surface air temperatures in Control **B-D**: Late-century (2090-2100) temperature changes with respect to the reference for Control, SAI 2020 and SAI 2080 respectively. **E**: Difference between SAI scenarios (**D** minus **C**)

3.2 AMOC Response

The AMOC index and meridional heat transport (MHT) roughly halve in Control (Fig. 3A-B). Even the CMIP6 low-emission SSP1-2.6 scenario is projected to lead to similar AMOC index changes. SAI 2020 drastically mitigates but does not halt the AMOC and MHT decline. SAI 2080 stabilizes the AMOC index but only has an inconclusive impact on the MHT.

Interestingly, SAI effectively decouples the GMST and the AMOC index (Fig. 3C). This could explain the interhemispheric temperature contrast featured in SAI 2080: a weak AMOC impedes northward heat transport leading to a see-saw temperature pattern (Stocker, 1998; Liu et al., 2020) that is not masked by heat otherwise present in Control.

To study the spatial pattern of the AMOC, we plot meridional streamfunction changes under all scenarios from 2070-2080 to 2090-2100 (Fig. 4). This choice of time intervals helps to reveal the immediate AMOC response to SAI 2080. Additionally, we subtract the changes in Control from the ones in the SAI scenarios in an attempt to disentangle GHG from SAI-related impacts.

Fig. 4D reveals a potential feedback in the AMOC stabilization under SAI 2080. Following the deployment, the pattern of relative AMOC strengthening closely mirrors the pre-deployment streamfunction, albeit mostly near the surface and in the northern hemisphere. This suggests that the AMOC response to abrupt SAI is dependent on the AMOC state itself. While a similar observation can be made for SAI 2020 (Fig. 4C), disentangling the forced response from internal feedback is not obvious during the gradual change in aerosol forcing. SAI 2080 gives a much better indication that it is indeed the state of the AMOC which steers its response to SAI.

This result again highlights the lack of immediate climate reversibility under SAI. A weakened AMOC state likely presents an obstacle to a SAI-based stabilization or recovery.

3.3 North Atlantic Deep Convection

We now focus on deep convection processes in the North Atlantic. Using mixed layer depth as a proxy for deep convection, we identify two regions, *East* and *West*, where the

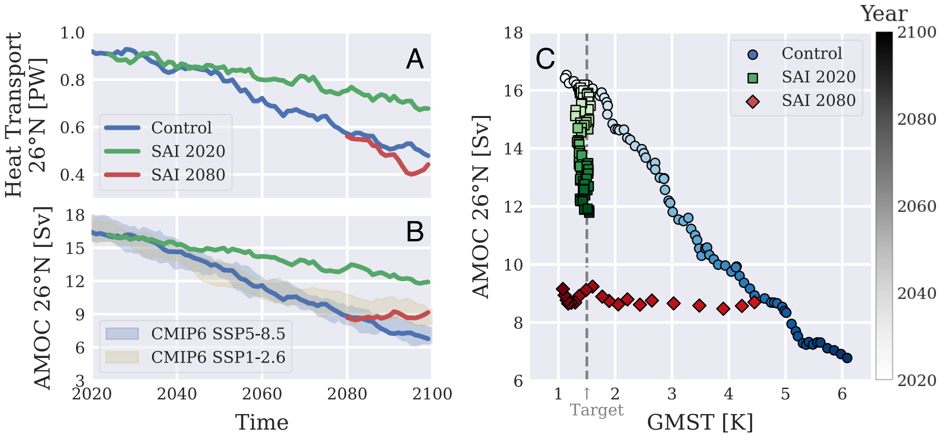

Figure 3. **A**: Annual mean Atlantic northwards heat transport at 26° N where we apply a rolling average over five year periods with backward window **B**: AMOC index defined as the maximum of the annual mean meridional overturning streamfunction at 26° N below 200 m - Partially transparent uncertainty bands depict three CESM2 CMIP6 ensemble members (Danabasoglu, 2019a, 2019b) per GHG concentration pathway. The uncertainty is the ensemble standard deviation. Again, we apply rolling averages over five year periods. **C**: Annual mean GMST vs. AMOC index - The marker saturation denotes the year: light (2020) to dark (2100).

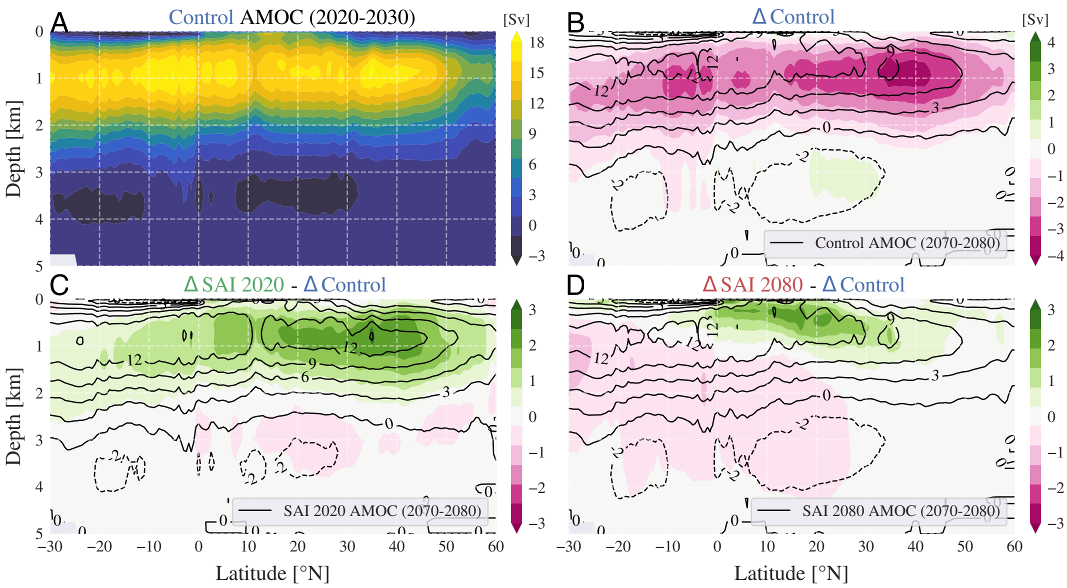

Figure 4. **A**: AMOC streamfunction in Control averaged over 2020-2030. In **B-D**, for any simulation X, Δ X is the mean over 2090-2100 minus the mean over 2070-2080. **B**: Change in AMOC streamfunction under Control - Black contour lines show the mean streamfunction over 2070-2080 for Control while the shading indicates Δ Control. **C**: Change in AMOC streamfunction in SAI 2020 relative to Control - Black contour lines show the mean streamfunction over 2070-2080 for SAI 2020 while the shading indicates Δ SAI 2020 - Δ Control. **D**: Analogous to **C** but for SAI 2080.

mixed layer depth in April (the month with the deepest mixed layer) exceeds 550 m (Fig. 5A). This threshold depth was chosen as it is sufficiently large to distinguish deep convection from regular mixed-layer conditions and small enough to provide a good signal-to-noise ratio. The regions are separated longitudinally by the southern tip of Greenland.

In Control, deep convection in *West* ceases around 2050, followed by a shutdown in *East* around 2060. SAI 2020 prevents the shutdown in *East*, but only postpones the shutdown in *West* by about a decade. The *West* shutdown is not as definite as in the case of Control and isolated years with deep convection still occur. For SAI 2080, deep convection remains absent in both regions with the exception of a single outlier year for *East*.

Why does cooling in SAI 2080 not revive deep convection? We address this question by studying the ocean stratification over both deep convection regions. Deep convection in April is inhibited if the surface density in the previous September has been too low, i.e. the water column is too stratified (Fig. S3). Thus, surface density serves as a proxy for favorable convection conditions.

The sea surface density is determined by temperature and salinity, also seen in Fig. 5. In all scenarios, final salinities are well below reference conditions. SAI 2020 roughly halves the decline with respect to Control. This difference becomes very noticeable mid-century simultaneously with the *East* and *West* shutdown in Control. SAI 2080 does not fundamentally alter the trajectory of Control apart from a transient increase in salinity that correlates with an isolated year of deep convection. Therefore, freshening contributes to density loss in all scenarios.

Temperature trends are rather complex in the case of Control (Fig. 5D-F.). An initial phase of slight cooling is interspersed with rapid, intense variability mid-century and finally succeeded by warming. Multiple factors like GHG-induced heating, cooling from a declining AMOC as well as convection related surfaces fluxes and currents overlap and are causing this behaviour.

SAI 2020 shows an overall cooling trend dominated by a quick decline at time of *West* shutdown. In SAI 2080, prior deep convection shutdown combined with SAI leads to drastic cooling even falling below SAI 2020 levels (Fig. 5D). These temperature drops have a positive effect on density and thereby convection. Still, the dramatic cooling in SAI 2080 does not elevate densities to SAI 2020 levels (Fig. 5F). Therefore, the salinity deficit of SAI 2080 with respect to SAI 2080 (Fig. 5E) presents a clear obstacle for restarting deep convection.

Our results can be explained in terms of multiple physical drivers. Firstly, all scenarios see an increase in surface freshwater forcing (Fig. S2) which contributes to a gradual salinity loss. This weakens convection and consequently the AMOC. Subsequently, weak AMOC and convection conditions lead to less salt transport into the subpolar gyre, hence reinforcing the salinity decline (Kuhlbrodt et al., 2007). This is particularly true for the late years of Control and SAI 2080. Finally, increasing the surface density via cooling has 'diminishing returns': density gains are less than proportional to temperature decreases owing to the nonlinear properties of sea water density. As shown in the supplementary material (Fig. S4), this further reduces the efficacy of SAI 2080.

To summarise, SAI 2020 partially stabilizes deep convection. In contrast, the salinity deficit accumulated up to deployment time in SAI 2080 becomes an obstacle for strengthening convection. There, the absence of positive convective feedback combined with a weak AMOC offers little hope of a decisive recovery but internal variability may still lead to isolated events of deep convection. It is not implausible that multiple such events could compound and eventually restore deep convection in the longer term.

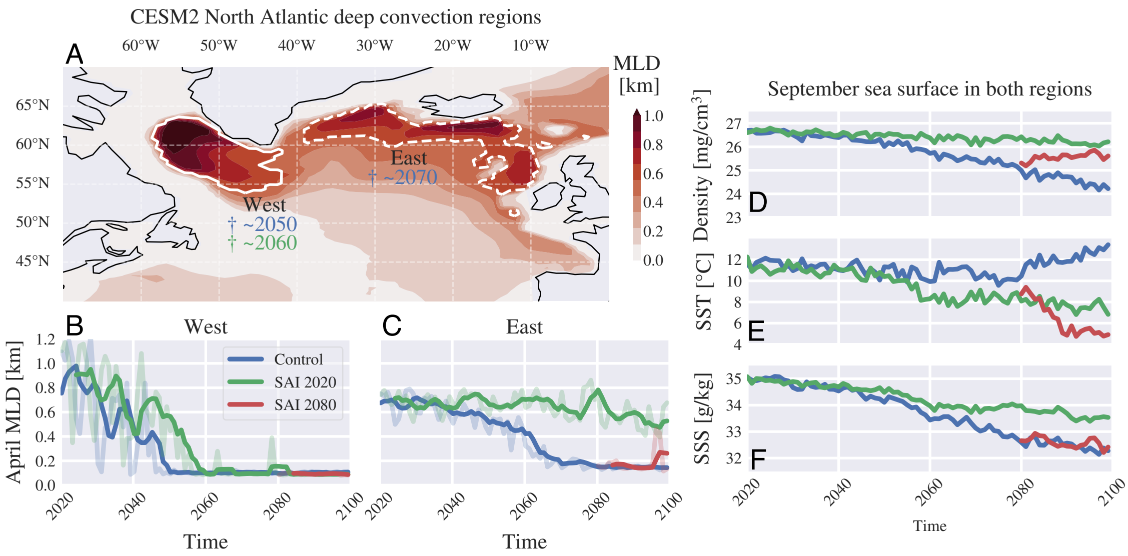

Figure 5. **A**: North Atlantic April mixed layer depths in CESM2 (2020-2030) - *East* and *West* are enclosed by solid and dashed lines respectively. Shutdown dates are denoted with a cross and colored according to scenario (blue: Control, green: SAI 2020). **B-C**: April mixed layer depths in *West* and *East* respectively - Solid lines are five year rolling means (with backward window) applied to the data shown by transparent lines. **D-F**: September mean sea surface density, temperature and salinity over the total *East* and *West* region

4 Discussion

In our simulations, the quick drop in GMST due to abrupt SAI is contrasted by a slow ocean response. Gradual SAI, on the other hand, retains an ocean state much closer to the present-day reference. Elevated OHC, weak AMOC and absent deep convection coupled with a lower GMST presents a (transient) climate state unknown from purely GHG-forced scenarios.

Note that our scenarios are extreme cases with a high signal-to-noise ratio, rather than desirable or plausible futures. More cautious protocols typically deploy SAI in tandem with emission mitigation to limit a temporary temperature overshoot (National Academies of Sciences, Engineering, and Medicine, 2021). If a cooling scenario were actually considered, a ramp-up of SAI would be more sensible than the sudden deployment in SAI 2080. Such a gradual approach would enable a fine-tuning of the injection scheme based on observations.

Besides the high forcings, our scenarios also involve a limited SAI scheme. As our implementation relies on a single degree of freedom, we can only meet a GMST target but not control other aspects of the temperature pattern. More control parameters, on the other hand, may be beneficial to prevent a interhemispheric temperature asymmetry which risks a displacement of the ITCZ (Broccoli et al., 2006; Bischoff & Schneider, 2016). Still, restoring the meridional temperature pattern in SAI 2080 would come with problems of its own: less cooling over the North Atlantic further endangers deep convection.

As for our results, a mitigating effect of SAI on AMOC decline was already known in multiple models (Tilmes et al., 2018, 2019; Xie et al., 2022) but not in the case of late-century abrupt deployment. Similarly, the impaired effectiveness of abrupt SAI on reducing OHC is a new result. To our knowledge, no studies have been performed on the effect of SAI on deep convection shutdown either. Regarding this aspect, model dependencies are certain as deep convection shutdown is not a universal phenomenon in CMIP6 (Swingedouw et al., 2021).

It is worth pointing out similarities between our abrupt SAI case and rapid negative emission scenarios (Schwinger et al., 2022). Removal of GHG after prolonged heating can lead to an interhemispheric temperature asymmetry if the timescale of extraction is shorter than that of the AMOC recovery. Therefore, the possibility of SAI to manage the interhemispheric temperature gradient is an advantage compared to GHG removal.

A major questions remains open: do the climates of both SAI scenarios eventually converge? This question cannot be answered without extending the simulations, which is outside the scope of this study. When extrapolating our results, the OHC difference is expected to lessen due to residual ocean warming in SAI 2020. Whether the gap fully closes may also depend on the AMOC and deep convection because of their impact on ocean heat uptake (Marshall & Zanna, 2014). As for deep convection, the aforementioned salinity deficit in SAI 2080 inhibits convergence of the SAI scenarios. Nevertheless, should some years of deep convection arise in SAI 2080 (e.g. as a result of natural variability), salt import would be strengthened, thereby improving long-term prospects for deep convection.

5 Summary

In this study, we presented model results of a late-century “emergency brake” SAI deployment that aims to restore surface temperatures under simultaneous GHG forcing. By comparing our findings with a gradual early-century SAI scenario, we show that abrupt late-century SAI is less effective at mitigating changes in OHC, the AMOC and North Atlantic deep convection.

Firstly, abrupt SAI failed to release heat trapped in deeper ocean layers. Even an early onset of SAI only mitigates but does not halt OHC accumulation. Both results are linked to slow ocean equilibration times.

Secondly, abrupt SAI partially stabilized a weakened AMOC, albeit not halting the decline of northward heat transport. Under earlier SAI, the AMOC decline is mitigated in both, volume and heat transport. As a result, the scenarios achieved drastically different AMOC states despite comparable GMST. A weaker AMOC may contribute to the observed overcooling of the northern hemisphere in the emergency brake scenario. This, in turn, may be relevant for the choice of injection pattern.

Thirdly, a shutdown of North Atlantic deep convection could not be reversed with rapid, SAI-induced cooling. We suspect that a weakened AMOC, absence of convective feedback, fresher surface conditions as well as non-linear properties of water density pose an obstacle for restarting deep convection. An early intervention, on the other hand, retains more salt in the North Atlantic, hence the partial stabilization of deep convection.

All these findings suggest that SAI is not an effective emergency brake. Ocean changes induced by anthropogenic climate change can persist despite a rapid lowering of GMST. That is why, if SAI were ever considered, its efficacy would be limited by the ocean changes already locked-in. To avoid facing the choice of whether and how to deploy SAI all together, further climate change must be mitigated by curbing GHG emissions.

6 Open Research

The code for our SAI protocol will be shared upon reasonable request.

The CMIP6 data used for comparison in Fig. 3 is publicly available (Danabasoglu, 2019a, 2019b).

Acknowledgments

We thank Daniele Visioni, Doug McMartin and Ben Kravitz for sharing their feedforward-feedback controller code, our colleague Michael Kliphuis for providing his AMOC stream-function tools, Simone Tilmes for providing CESM2-WACCM data. Furthermore, we thank Jasper de Jong and Michiel Baatsen for fruitful discussions on the feedback control of SAI 2080.

References

Barrett, S., Lenton, T. M., Millner, A., Tavoni, A., Carpenter, S., Anderies, J. M., . . . De Zeeuw, A. (2014). Climate engineering reconsidered. *Nature Climate Change*. doi: 10.1038/nclimate2278

Biermann, F., Oomen, J., Gupta, A., Ali, S. H., Conca, K., Hajer, M. A., . . . Van-Deveer, S. D. (2022). Solar geoengineering: The case for an international non-use agreement. *WIREs Climate Change*. doi: 10.1002/wcc.754

Bischoff, T., & Schneider, T. (2016). The equatorial energy balance, ITCZ position, and double-ITCZ bifurcations. *Journal of Climate*. doi: 10.1175/JCLI-D-15-0328.1

Broccoli, A. J., Dahl, K. A., & Stouffer, R. J. (2006). Response of the ITCZ to northern hemisphere cooling. *Geophysical Research Letters*. doi: 10.1029/2005GL024546

Buck, H. J. (2019). *After geoengineering: climate tragedy, repair, and restoration.* Verso.

Cheng, L., Von Schuckmann, K., Abraham, J. P., Trenberth, K. E., Mann, M. E., Zanna, L., . . . Lin, X. (2022). Past and future ocean warming. *Nature Reviews Earth & Environment*. doi: 10.1038/s43017-022-00345-1

Crutzen, P. J. (2006). Albedo enhancement by stratospheric sulfur injections: A contribution to resolve a policy dilemma? *Climatic Change*. doi: 10.1007/s10584-006-9101-y

Danabasoglu, G. (2019a). *NCAR CESM2 model output prepared for CMIP6 ScenarioMIP ssp370.* Earth System Grid Federation. doi: 10.22033/ESGF/CMIP6.7753

Danabasoglu, G. (2019b). *NCAR CESM2 model output prepared for CMIP6 ScenarioMIP ssp585.* Earth System Grid Federation. doi: 10.22033/ESGF/CMIP6.7768

Danabasoglu, G., Lamarque, J., Bacmeister, J., Bailey, D. A., DuVivier, A. K., Edwards, J., . . . Strand, W. G. (2020). The community earth system model version 2 (CESM2). *Journal of Advances in Modeling Earth Systems*. doi: 10.1029/2019MS001916

Drijfhout, S., van Oldenborgh, G. J., & Cimatoribus, A. (2012). Is a decline of AMOC causing the warming hole above the north atlantic in observed and modeled warming patterns? *Journal of Climate*. doi: 10.1175/JCLI-D-12-00490.1

Fasullo, J. T., Tilmes, S., Richter, J. H., Kravitz, B., MacMartin, D. G., Mills, M. J., & Simpson, I. R. (2018). Persistent polar ocean warming in a strategically geoengineered climate. *Nature Geoscience*. doi: 10.1038/s41561-018-0249-7

Florin, M.-V., Rouse, P., Hubert, A.-M., Honegger, M., & Reynolds, J. (2020). lnternational governance issues on climate engineering information for policymakers. doi: 10.5075/EPFL-IRGC-277726

Hassan, T., Allen, R. J., Liu, W., & Randles, C. A. (2021). Anthropogenic aerosol forcing of the atlantic meridional overturning circulation and the associated mechanisms in CMIP6 models. *Atmospheric Chemistry and Physics*. doi: 10.5194/acp-21-5821-2021

IPCC. (2022a). *Climate change 2022: Impacts, adaptation and vulnerability.* Cambridge University Press. doi: 10.1017/9781009325844

IPCC. (2022b). *Climate change 2022: Mitigation of climate change.* Cambridge University Press.

Irvine, P., Emanuel, K., He, J., Horowitz, L. W., Vecchi, G., & Keith, D. (2019). Halving warming with idealized solar geoengineering moderates key climate hazards. *Nature Climate Change*. doi: 10.1038/s41558-019-0398-8

Kleinschmitt, C., Boucher, O., & Platt, U. (2018). Sensitivity of the radiative forcing by stratospheric sulfur geoengineering to the amount and strategy of the SO_2 injection studied with the LMDZ-S3A model. *Atmospheric Chemistry and Physics*. doi: 10.5194/acp-18-2769-2018

Kravitz, B., MacMartin, D. G., Mills, M. J., Richter, J. H., Tilmes, S., Lamarque, J., ... Vitt, F. (2017). First simulations of designing stratospheric sulfate aerosol geoengineering to meet multiple simultaneous climate objectives. *Journal of Geophysical Research: Atmospheres*. doi: 10.1002/2017JD026874

Kravitz, B., MacMartin, D. G., Wang, H., & Rasch, P. J. (2016). Geoengineering as a design problem. *Earth System Dynamics*. doi: 10.5194/esd-7-469-2016

Kuhlbrodt, T., Griesel, A., Montoya, M., Levermann, A., Hofmann, M., & Rahmstorf, S. (2007). On the driving processes of the atlantic meridional overturning circulation. *Reviews of Geophysics*.

Liu, W., Fedorov, A. V., Xie, S.-P., & Hu, S. (2020). Climate impacts of a weakened atlantic meridional overturning circulation in a warming climate. *Science Advances*. doi: 10.1126/sciadv.aaz4876

Lockley, A., Xu, Y., Tilmes, S., Sugiyama, M., Rothman, D., & Hindes, A. (2022). 18 politically relevant solar geoengineering scenarios. *Socio-Environmental Systems Modelling*. doi: 10.18174/sesmo.18127

MacMartin, D. G., Kravitz, B., Tilmes, S., Richter, J. H., Mills, M. J., Lamarque, J., ... Vitt, F. (2017). The climate response to stratospheric aerosol geoengineering can be tailored using multiple injection locations. *Journal of Geophysical Research: Atmospheres*. doi: 10.1002/2017JD026868

Marshall, D. P., & Zanna, L. (2014). A conceptual model of ocean heat uptake under climate change. *Journal of Climate*. doi: 10.1175/JCLI-D-13-00344.1

Menary, M. B., & Wood, R. A. (2018). An anatomy of the projected north atlantic warming hole in CMIP5 models. *Climate Dynamics*. doi: 10.1007/s00382-017-3793-8

National Academies of Sciences, Engineering, and Medicine. (2021). *Reflecting sunlight: Recommendations for solar geoengineering research and research governance.* National Academies Press. doi: 10.17226/25762

Oomen, J. (2021). *Imagining climate engineering: dreaming of the designer climate.* Routledge, Taylor & Francis Group.

Plazzotta, M., Séférian, R., Douville, H., Kravitz, B., & Tjiputra, J. (2018). Land surface cooling induced by sulfate geoengineering constrained by major volcanic eruptions. *Geophysical Research Letters*. doi: 10.1029/2018GL077583

Schwinger, J., Asaadi, A., Goris, N., & Lee, H. (2022). Possibility for strong northern hemisphere high-latitude cooling under negative emissions. *Nature Communications*. doi: 10.1038/s41467-022-28573-5

Sgubin, G., Swingedouw, D., Drijfhout, S., Mary, Y., & Bennabi, A. (2017). Abrupt cooling over the north atlantic in modern climate models. *Nature Communications*. doi: 10.1038/ncomms14375

Smith, W. (2020). The cost of stratospheric aerosol injection through 2100. *Environmental Research Letters*. doi: 10.1088/1748-9326/aba7e7

Stocker, T. F. (1998). The seesaw effect. *Science*. doi: 10.1126/science.282.5386.61

Svoboda, T. (2017). *The ethics of climate engineering: solar radiation management and non-ideal justice.* Routledge, Taylor & Francis Group.

Swingedouw, D., Bily, A., Esquerdo, C., Borchert, L. F., Sgubin, G., Mignot, J., & Menary, M. (2021). On the risk of abrupt changes in the north atlantic subpolar gyre in CMIP6 models. *Annals of the New York Academy of Sciences*. doi: 10.1111/nyas.14659

Tilmes, S., MacMartin, D. E., Lenaerts, J. T. M., Van Kampenhout, L., Muntjewerf, L., Xia, L., … Robock, A. (2019). Reaching 1.5 °c and 2.0 °c global surface temperature targets using stratospheric aerosol geoengineering [preprint]. *Earth System Dynamics*. doi: 10.5194/esd-2019-76

Tilmes, S., Richter, J. H., Kravitz, B., MacMartin, D. G., Mills, M. J., Simpson, I. R., … Ghosh, S. (2018). CESM1(WACCM) stratospheric aerosol geoengineering large ensemble project. *Bulletin of the American Meteorological Society*. doi: 10.1175/BAMS-D-17-0267.1

Wieners, C. E., Hofbauer, B. P., De Vries, I. E., Honegger, M., Visioni, D., Russchenberg, H. W. J., & Felgenhauer, T. (2023). Solar radiation modification is risky, but so is rejecting it: a call for balanced research. *Oxford Open Climate Change*. doi: 10.1093/oxfclm/kgad002

Xie, M., Moore, J. C., Zhao, L., Wolovick, M., & Muri, H. (2022). Impacts of three types of solar geoengineering on the atlantic meridional overturning circulation. *Atmospheric Chemistry and Physics*. doi: 10.5194/acp-22-4581-2022

Supplementary Material: No Emergency Brake: Slow Ocean Response to Abrupt Stratospheric Aerosol Injection

Daniel Pflüger[1], Claudia E. Wieners[1], Leo van Kampenhout[1], René R. Wijngaard[1], and Henk A. Dijkstra[1]

[1]Institute Marine and Atmospheric Research Utrecht, Princetonplein 5, 3584 CC Utrecht, The Netherlands

August 28, 2023

Variable name	Description	Normalization
AODVISstdn	Aerosol optical depth	Global mean
SAD_AERO	Surface aerosol density	Total aerosol surface area
so4mass_a1	Aerosol mass concentration of aerosol mode one	Total mass
so4mass_a2	Aerosol mass concentration of aerosol mode two	Total mass
so4mass_a3	Aerosol mass concentration of aerosol mode three	Total mass
diamwet_a1	Aerosol wet diameter of aerosol mode one	Root mean square
diamwet_a2	Aerosol wet diameter of aerosol mode second	Root mean square
diamwet_a3	Aerosol wet diameter of aerosol mode three	Root mean square

Table 1: Prescribed aerosol fields in CESM2-CAM6 with description of respective normalizing approach

1 Methods

1.1 Prescribed aerosols

Our SAI implementation is based on prescribed aerosol fields. This means that the variables representing stratospheric aerosols are predetermined, non-interactive and serve as boundary conditions for CAM6. To achieve this, we process stratospheric aerosol variables obtained by CESM2-WACCM simulations [4].

Let $F^{\text{in}}(t,d,x)$ be an CESM2-WACCM stratospheric aerosol field at year t, day of the year d and position x (e.g. longitude, latitude, altitude or a combination thereof). We process this field in three steps: normalization, averaging and fitting.

Firstly, we apply a normalization to the field. The choice of normalization depends on the type of field and can either be physically motivated or mathematically practical, see also Table 1. In any case, we obtain a norm $n(t)$ of $F^{\text{in}}(t,d,x)$ for any given year. This also gives a normalized field $\hat{F}^{\text{in}}(t,d,x) = \frac{1}{t_f - t_i} F^{\text{in}}(t,d,x)/n(t)$ The normalized field predominantly carries information about the spatial and seasonal distribution of the aerosol field. Its amplitude, however, is removed in this step.

Secondly, we average the normalized field over multiple years. In our case, we decided to use the years 2070-2100 in which the CESM2-WACCM simulations attain large aerosol burdens and potentially provide a more accurate starting point for our SAI 2080 scenario. The averaging yields $\bar{F}(d,x) = \sum_{t=t_i}^{t_f} \hat{F}^{\text{in}}(t,d,x)$.

After performing these steps for all fields, i.e. obtaining $\bar{F}_i(d,x)$ and $n_i(t)$ for every field with index i, we designate one field as the reference. We choose the global mean aerosol optical depth (AOD) as it intuitively provides the overall level of shading. For simplicity, we will denote this field and its normalization constant as $\bar{F}(d,x)$ and $n(t)$ without the index i. We then individually fit all normalization constants n_i against n using a power-law ansatz. This yields fits $n_i^f(n)$ dependent on n.

As a final result, we can compute the prescribed fields $F_i(t,d,x)$ using only $n(t)$ and the averaged fields $F_i(d,x)$ as an input:

$$F_i(t,d,x) = n_i^f(n(t)) F_i(d,x) \tag{1}$$

Note that the main parameter n itself has to be dynamically adjusted to maintain a desired temperature target. That is the goal of the feedback-feedforward controller.

Our approach can be validated twofold. Firstly, a ‘dry-run’ can be performed by using stratospheric aerosol data $F_i^{\text{in}}(t,d,x)$ from a WACCM run. The input AOD time series $n^{\text{in}}(t)$ is then used to generate prescribed fields $F_i(t,d,x)$ which can finally be compared to $F_i^{\text{in}}(t,d,x)$, e.g. by computing a specified norm $||F_i - F_i^{\text{in}}||$. This essentially tests the ability of the scaling algorithm to reconstruct the original WACCM fields. Secondly, by

Scenario	k_{ff}	t_{ff}	k_{p}	k_{i}
SAI 2020	0.0103	2020	0.028	0.028
SAI 2080	0.0096	2028	0.028	0.028
SAI 2080 (mod)	0.0096	2028	0.028	0.028

Table 2: Feedforward-feedback parameters for all scenarios assuming that time is given in units of years and temperature in units of Kelvin.

performing a feedback-feedforward controlled run with the same temperature target and GHG forcing as an available WACCM run, one can test if the physical output of CESM2 behaves in a similar way. The validation of our approach is part of a publication currently in preparation.

1.2 Feedback-Feedforward Algorithm

We control the GMST by adjusting the aerosol shading, parameterised by the AOD n. For that purpose, we use a feedback-feedforward algorithm that has become common in SAI modelling.

The algorithm starts from an informed guess of the expected AOD necessary for a specific level of cooling. This so-called feedforward could for example come from estimates of aerosol sensitivity of radiative forcing [2]. In our case, we use tweaked estimates from aforementioned CESM2-WACCM runs.

On top of the feedforward, proportional-integral feedback adds a correction based on the deviation $\Delta T(t)$ of the GMST from the target. As their names suggest, the proportional and integral components of the feedback introduce corrections directly proportional to $\Delta T(t)$ as well as proportional to the discrete sum $\sum_{t'=t_i}^{t} \Delta T(t')$.

In total, the AOD $n(t)$ in year t is

$$n(t) = \underbrace{k_{\mathrm{ff}}(t - t_{\mathrm{ff}})}_{\text{feedforward}} + \underbrace{k_{\mathrm{p}}\Delta T(t)}_{\text{proportional}} + \underbrace{k_{\mathrm{i}} \sum_{t'=t_i}^{t} \Delta T(t')}_{\text{integral}} \tag{2}$$

where $k_{\mathrm{ff}}, k_{\mathrm{p}}, k_{\mathrm{i}}$ and t_{ff} are constants.

Under SAI 2020, the integrator is simply initialized in $t_{\mathrm{i}} = 2020$. To avoid a large integral term - an 'integrator windup' [1] - during cooling in SAI 2080, we have considered multiple options but acknowledge that there is a substantial freedom of choice. In SAI 2080, the integrator term is activated conditionally either six years after SAI 2080 deployment or when stabilizing temperatures within 0.5K around the target. In a modified scenario - SAI 2080 (mod) - the integrator is turned on from the start but resets when the temperature target is crossed.

Note that the feedforward was adjusted when going from SAI 2020 to SAI 2080, see also Table 2. The updated parameters were obtained by using the output of the trained SAI 2020 feedforward-feedback controller.

2 GMST and AOD

Fig. S1 shows how the modified integrator in SAI 2080 (mod) resolves the issue of overcooling. Unfortunately, the AOD calculated by the feedforward-feedback controller has a substantial discontinuity at the time of integrator reset. In principle, the transiently high

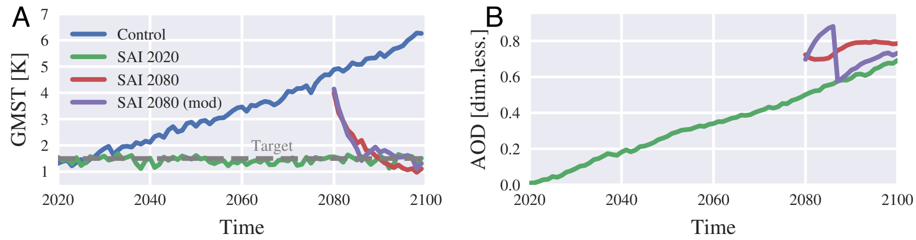

Figure S 1: **A**: Annual mean GMST for all scenarios from main text with addition of modified SAI 2080 scenario **B**: Global and annual mean stratospheric aerosol optical depth in all SAI scenarios (including modified SAI 2080 scenario)

AOD induces changes in freshwater fluxes and we can not rule out unexpected effects on the oceans. For that reason, we focused only on the original SAI 2080.

Ultimately, there is a freedom of choice in the cooling scenario. A longer cooling period could lower the aerosol burden in the transition period but likely worsen the signal-to-noise ratio of the climate response. As our SAI 2080 scenario is only understood to be a physical edge case, we did not implement a longer cooldown.

3 Surface Freshwater Fluxes in Deep Convection Regions

Multiple drivers are responsible for fresher conditions in deep convection regions. While we have not disentangled all possible contributions, we can rule out surface freshwater flux (SFWF) being the distinguishing feature between scenarios. SFWF consists of precipitation, evaporation, sea ice melt/growth and runoff terms. Fig. S2 shows that SFWF increases in all scenarios. While Control and SAI 2020 have similar values throughout the simulation, SAI 2080 induces slightly fresher conditions.

The remarkably similar SFWF are unexpected because SAI has a distinct impact on the hydrological cycle (Fig. S2B-C). The decline in atmospheric freshwater flux turns out to be compensated by increased sea ice melting (Fig. S2D). Apparently, the cool SAI conditions allow for sea ice import and subsequent melting in the deep convection regions. The negative residual fluxes at the end of Control are an artefact of the implementation of ice runoff fluxes in the land model [3, Ch. 13.5, p. 145].

4 Stratification and Mixed Layer

The deep convection season in the North Atlantic depends on a pre-conditioning, i.e. a weak stratification after summer. Fig. S3 makes it clear that high sea surface densities (here used as a proxy for stratification) in September correlate with deep mixed layers in the following April. More specifically, deep convection is enabled for sea surface densities beyond a critical value of around 26 mg/cm^3. Beyond that point, there is a large, internal variability in mixed layer depths.

Fig. S4 explains the sea surface density dynamics in terms of temperature and salinity. We see that salinities in *West* fall enough to place both, SAI 2020 and SAI 2080, well below the critical density. In *East*, SAI 2020 manages to stay above the critical threshold as cooling balances the effects of freshening. Branching off from Control, SAI 2080 experiences a cooling shock that brings densities very close to the line of critical density.

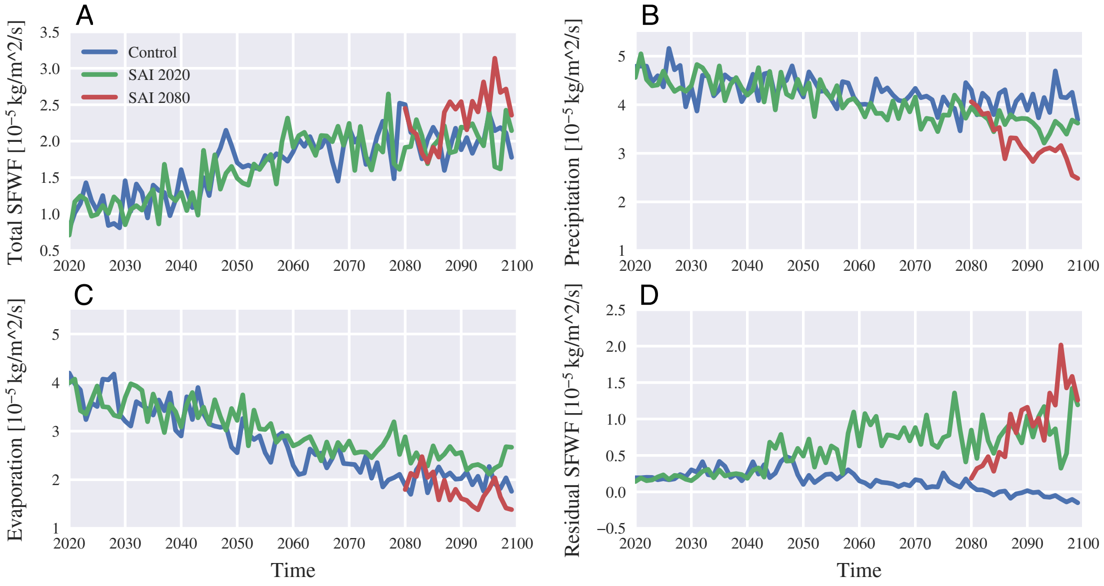

Figure S 2: Mean annual surface freshwater fluxes into total *East* and *West* regions; positive values indicate downward flux except for **C** - **A**: Total flux **B**: Precipitation **C**: Evaporation **D**: Residual = Total flux - (Precipitation - Evaporation); contains sea ice contributions

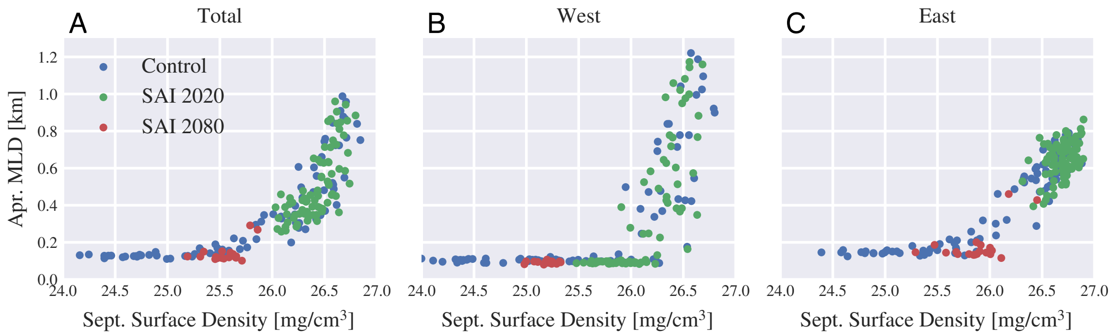

Figure S3: **A-C** April mixed layer depth versus surface density of previous September in respective regions - The density values have an offset of $1000\,\mathrm{mg/cm^3}$.

Note that the lines of equal density in Fig. S4 are convex which is a consequence of the nonlinear equation of state for sea water. The thermal expansivity of water decreases with lower temperatures: the cooler the initial temperature, the weaker the density gain for any given temperature drop. If the equation of state were linear, (i.e. density depending linearly on temperature and salinity) abrupt cooling could have restarted deep convection in *East*.

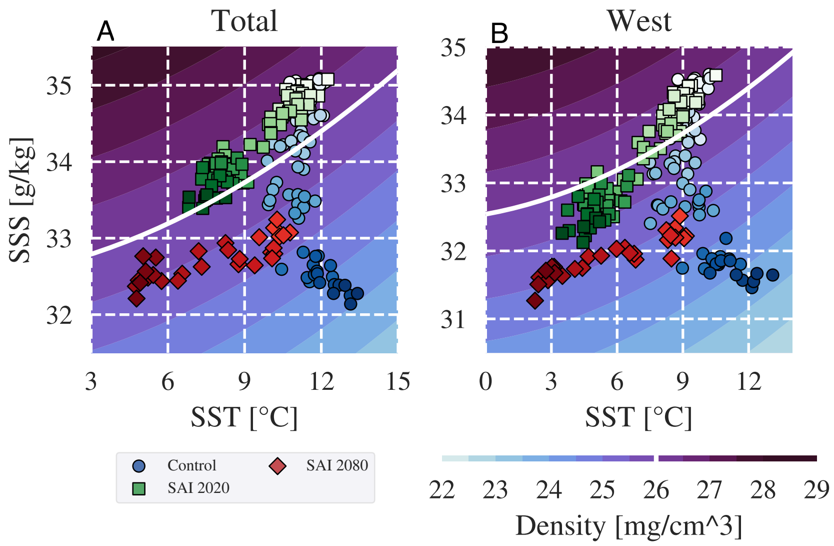

Figure S4: **A-C**: Sea surface salinity and temperature trajectories in all respective regions - Filled contours represent the water density. The singled out white contour is at the critical density of 26 mg/cm^3. Marker saturation represents time and ranges from light (2020) to saturated (2100).

References

[1] Karl Johan Astrom and Lars Rundqwist. Integrator windup and how to avoid it. In *1989 American Control Conference*. IEEE, 1989.

[2] James Hansen, MKI Sato, R Ruedy, L Nazarenko, A Lacis, GA Schmidt, G Russell, I Aleinov, M Bauer, S Bauer, et al. Efficacy of climate forcings. *Journal of Geophysical Research: Atmospheres*, 2005.

[3] David Lawrence, Rosie Fisher, Charles Koven, Keith Oleson, Sean Swenson, Mariana Vertenstein, et al. Technical description of version 5.0 of the community land model (clm). Technical report, National Center for Atmospheric Research, February 2018.

[4] Simone Tilmes, Douglas E. MacMartin, Jan T. M. Lenaerts, Leo Van Kampenhout, Laura Muntjewerf, Lili Xia, Cheryl S. Harrison, Kristen M. Krumhardt, Michael J. Mills, Ben Kravitz, and Alan Robock. Reaching 1.5 °C and 2.0 °C global surface temperature targets using stratospheric aerosol geoengineering, 2019.